Three-Dimensional Computations of the Impulsive Wave Discharged from a Duct

Young-Ki Lee
School of Mechanical Engineering, Andong National University,
388 Songcheon-dong, Andong 760-749, Korea

Yong-Hun Kweon
Department of Energy and Environmental Engineering, Kyushu University,
6-1, Kasugakouen, Kasuga, Fukuoka, 816-8580, Japan

Heuy-Dong Kim*
School of Mechanical Engineering, Andong National University,
388 Songcheon-dong, Andong 760-749, Korea

Toshiaki Setoguchi
Department of Mechanical Engineering, Saga University,
1, Honjo-machi, Saga, 840-8502, Japan

A sudden discharge of mass flow from the exit of a duct can generate an impulsive wave, generally leading to undesirable noise and vibration problems. The present study develops an understanding of unsteady flow physics with regard to the impulsive wave discharged from a duct, using a numerical method. A second order total variation diminishing scheme is employed to solve three-dimensional, unsteady, compressible Euler equations. Computations are performed for several exit conditions with and without ground and wall effects under a change in the Mach number of an initial shock wave from 1.1 to 1.5. The results obtained show that the directivity and magnitude of the impulsive wave discharged from the duct are significantly influenced by the initial shock Mach number and by the presence of the ground and walls.

Key Words : Compressible Flow, Ground Effect, Impulsive Noise, Unsteady Flow, Wave Propagation, Weak Shock Wave

Nomenclature

a : Speed of sound
e : Total energy per unit volume
H : Hydraulic diameter of a duct
M_s : Mach number of an initial shock wave
p : Static pressure
t : Time
u,v,w : Velocity components in the x-, y- and z-directions

x,y,z : Cartesian coordinates
Δp_{max} : Peak pressure measured from the atmospheric pressure level
Δt : Time interval
Δx : Grid space in the x-direction
γ : Specific heat ratio
θ : Azimuth angle (deg.)
ρ : Density

Sub/superscripts

i,j,k : Space nodes in the x-, y- and z-directions
n : Time step
0 : Atmospheric state
$'$: Non-dimensional value

* Corresponding Author,
  E-mail : kimhd@andong.ac.kr
  TEL : +82-54-820-5622; FAX : +82-54-823-5495
  School of Mechanical Engineering, Andong National University, 388 Songcheon-dong, Andong 760-749, Korea. (Manuscript **Received** July 16, 2004; **Revised** December 3, 2004)

1. Introduction

A compression wave propagating in tubes, ducts, piping systems, etc. can produce an impulsive wave when it is suddenly discharged from their open ends. This phenomenon can be encountered in a variety of unsteady internal flow devices such as gun muzzles (Klingenberg and Heimerl, 1992), internal combustion engine exhaust mufflers (Sekine et al., 1989), dynamic pressure exchangers (Kentfield, 1993), pulse combustors (Zinn, 1985), high-speed railway train / tunnel system (Ozawa et al., 1991 ; Matsuo and Aoki, 1992), and pulse jet filters (Klingel and Löffler, 1983). In addition, pressure transients occur inside a flow passage due to the successive reflection of pressure waves generated between the entrance and exit of the passage (Fox and Vardy, 1973). Both the impulsive wave and pressure transients generally cause severe noise and vibration problems.

A pressure wave generated inside a duct propagates through the duct at a speed depending on the amplitude of the pressure wave and local flow conditions. As the pressure wave arrives at an open end of the duct and discharges toward the surroundings, it should meet the boundary conditions given at the duct exit. The open-end boundary conditions usually require two kinds of wave systems (Rudinger, 1955 ; Rudinger, 1957), a reflected expansion wave propagating back from the open end of the duct and a discharged pressure wave propagating into the surroundings. In general, the reflected expansion wave causes pressure transients inside the duct while the discharged pressure wave is attenuated into a pulse-like impulsive wave outside the duct.

An impulsive wave is usually characterised by a high sound pressure level during short time and propagates far away from the duct exit (Raghunathan et al., 1998). This can cause human beings as well as flow devices to face a serious noise problem and the reduction of the noise is, therefore, an important consideration to improve the performance of the flow devices. The characteristics of the impulsive wave have

traditionally been examined by using the linear acoustics of an infinitesimal amplitude wave, usually with the hypotheses of negligible non-linear effects and directional sensitivity of the impulsive wave (Setoguchi et al., 1993). In this manner, some reports have been made on the blast wave resulting from a strong shock discharged from a tube exit (Pennelegion and Grimshaw, 1979 ; Britan et al., 1988 ; Cooke and Fansler ; 1989). However, the impulsive wave that can often be encountered in a number of engineering applications has a character of a typical weak shock wave and only a few researches (Kim et al., 2003b) have been carried out on this problem.

Recently, Kim and Setoguchi (1998), and Kim et al.(1999) performed some experiments using an open-ended shock tube and computations using a TVD (total variation diminishing) scheme. The impulsive wave generated by the discharge of a weak shock was characterised in terms of the peak pressure, open-end correction, directional sensitivity, and attenuation with the propagating distance. Their ensuing experimental research (Kim et al., 2004) showed that the control technique using a cavity/helical vane system reduced the peak pressure of the impulsive wave up to about 50% in comparison with a straight tube and, thus, it was suitable for alleviating the magnitude of the impulsive wave.

Most of researches on this topic have been conducted regarding an impulsive wave discharged from a fully open exit configuration. Actually, however, the circumstance near the exit of pulse devices such as high-speed railway tunnels is often under ground effects or influenced by other objects placed in the vicinity of the exit. Therefore, the characteristics of the impulsive wave may not be clearly understood only through the results established so far.

The main aim of the present study is to clarify the influence of the ground or some objects placed in the near field of a discharging flow from the exit of a duct on the propagation of an impulsive wave towards the surroundings. Euler computations were conducted for three-dimensional, unsteady, inviscid, compressible flow fields, using a TVD scheme. Concerning a basic exit configu-

ration of the duct, fully open towards the atmosphere, the objects affecting the impulsive wave propagation were set up with three different types of configurations, including a ground, ground-wall and ground-walls. The results obtained through the computations are compared with available experimental data (Jiang et al., 1999) and the visualisation of the wave propagation is also presented in this paper.

2. Numerical Simulations

2.1 Governing equations

In order to simulate three-dimensional, unsteady, inviscid, compressible flows characterised by the propagation of an impulsive wave, Euler equations are employed in the present study. The governing conservation equations are given in differential form as follows :

$$\frac{\partial U}{\partial t}+\frac{\partial E}{\partial x}+\frac{\partial F}{\partial y}+\frac{\partial G}{\partial z}=0 \qquad (1)$$

where

$$U=\begin{bmatrix} \rho \\ \rho u \\ \rho v \\ \rho w \\ e \end{bmatrix}, E=\begin{bmatrix} \rho u \\ \rho u^2+p \\ \rho uv \\ \rho uw \\ (e+p)u \end{bmatrix}, F=\begin{bmatrix} \rho v \\ \rho uv \\ \rho v^2+p \\ \rho vw \\ (e+p)v \end{bmatrix}, G=\begin{bmatrix} \rho w \\ \rho uw \\ \rho vw \\ \rho w^2+p \\ (e+p)w \end{bmatrix}$$

and u, v and w are the velocity components in the x-, y- and z-directions, respectively. The total energy e per unit volume of a perfect gas is expressed as $e=p/(\gamma-1)+\rho(u^2+v^2+w^2)/2$. In computations, Eq. (1) is rewritten in non-dimensional form by referring the quantities such as pressure, density, etc. at atmospheric conditions and the hydraulic diameter of a duct, as given below :

$$t'=\frac{t}{(H/a_0)\sqrt{\gamma}}, \; x'=\frac{x}{H}, \; y'=\frac{y}{H}, \; z'=\frac{z}{H},$$

$$p'=\frac{p}{p_0}, \; \rho'=\frac{\rho}{\rho_0}, \; u'=\frac{u}{a_0/\sqrt{\gamma}}, \qquad (2)$$

$$v'=\frac{v}{a_0/\sqrt{\gamma}}, \; w'=\frac{w}{a_0/\sqrt{\gamma}}$$

where the superscript ($'$) and subscript 0 indicate non-dimensionalized values and the atmospheric condition, respectively, H is the hydraulic diameter, and a is the speed of sound.

2.2 Numerical scheme

TVD schemes have been known to be very effective for computing the phenomena of shock waves without presenting spurious oscillations, which are often associated with conventional second-order schemes in the presence of discontinuities. For the present computational analysis, the Yee-Roe-Davis's TVD scheme (Yee, 1987) is employed to discretise governing equations. For the computation of time-dependent flows, an operator splitting technique, which was suggested by Sod (1977), is used for temporal and spatial derivatives, and then Eq. (1) can be given by a set of one-dimensional equations :

$$L_x:\frac{\partial U}{\partial t}+\frac{\partial E}{\partial x}=0, \; L_y:\frac{\partial U}{\partial t}+\frac{\partial F}{\partial y}=0,$$

$$L_z:\frac{\partial U}{\partial t}+\frac{\partial G}{\partial z}=0 \qquad (3)$$

$$U_{i,j,k}^{n+2}=L_xL_yL_zL_zL_yL_xU_{i,j,k}^n \qquad (4)$$

$$L_xU_{i,j,k}^n=U_{i,j,k}^{n+1}=U_{i,j,k}^n-\frac{\Delta t}{\Delta x}[\hat{E}_{i+1/2}^n-\hat{E}_{i-1/2}^n] \; (5)$$

where the subscripts i, j and k and the superscript n indicate the space nodes and time step, and L_x, L_y and L_z are the differential operators for the x-, y- and z-directions, respectively. In Eq. (5), Δt and Δx indicate the time interval and the grid space in the x-direction, and $\hat{E}$ denotes the numerical flux in the x-direction, which is given by

$$\hat{E}_{i+1/2}^n=\frac{1}{2}[E_i^n+E_{i+1}^n+R_{i+1/2}^n\cdot\varPhi_{i+1/2}^n] \qquad (6)$$

where $R_{i+1/2}^n$ is a matrix whose column vectors are the right eigenvectors of the flux Jacobian $\partial F/\partial U$, evaluated by a symmetric average of $U_{i,j,k}$ and $U_{i+1,j,k}$. The last term $R_{i+1/2}^n\cdot\varPhi_{i+1/2}^n$ represents the anti-diffusive flux contribution that corrects the excessive dissipation of first-order numerical flux in a nonlinear way. The numerical flux vectors in the y- and z-directions, $\hat{F}_{j+1/2}^n$ and $\hat{G}_{k+1/2}^n$, can be similarly expressed.

For Yee-Roe-Davis's second-order symmetric TVD scheme, the vector $\Phi_{i+1/2}^{n}$ is given as

$$\Phi_{i+1/2}=-\left[\frac{\Delta t}{\Delta x}(a_{i+1/2})^2 g_{i+1/2}+\psi(a_{i+1/2})(\alpha_{i+1/2}-g_{i+1/2})\right] \quad (7)$$

where $a_{i+1/2}$ is the eigen-value of the flux Jacobian matrix in the x-direction, $\alpha_{i+1/2}$ is the forward difference of the local characteristic variables in the x-direction, and $g_{i+1/2}$ is a limiter function. $\alpha_{i+1/2}$ and $g_{i+1/2}$ are defined as follows:

$$\alpha_{i+1/2}=R_{i+1/2}^{-1}\cdot(U_{i+1,j}-U_{i,j}) \quad (8)$$

$$g_{i+1/2}=\text{min mod }(\alpha_{i-1/2}, \alpha_{i+1/2}, \alpha_{i+3/2}) \quad (9)$$

The function $\psi(a_{i+1/2})$, called an entropy correction function, is defined as

$$\psi(a_{i+1/2})=\begin{cases} |a_{i+1/2}|, \text{ if } |a_{i+1/2}|\geq\varepsilon \\ (a_{i+1/2}^2+\varepsilon^2)/2\varepsilon, \text{ if } |a_{i+1/2}|<\varepsilon \end{cases} \quad (10)$$

where ε is a small positive number. This function corrects entropy to prevent it from violating solutions, such as expansion shock waves. The TVD scheme has been validated well with various physics regarding impulsive wave propagation through the authors' previous researches (Kim et al., 2003a; Kweon et al., 2003).

2.3 Computational domain and analysis

Figure 1 shows the testing exit configurations of a duct with and without walls placed in the near field downstream of the duct, aligned with the duct axis. The duct exit of Case 1 is fully open towards the atmosphere, and it is used for the basic configuration for the comparison with the others. Case 2, Case 3 and Case 4 include an exit with the ground, walls and sidewall, respectively. The ground and sidewall are in contact with the duct while the walls of Case 3, except the ground, surround the flow field.

In Fig. 2, the computational domain is shown with the boundary conditions applied to Case 1 for instance. The entire domain comprises solid boundaries forming a square cross-sectional duct with a width and height of H and a length of $3H$, and an outflow region (atmosphere) with dimensions of $4H\times7H\times7H$. Inflow and outflow conditions are applied to the duct inlet and
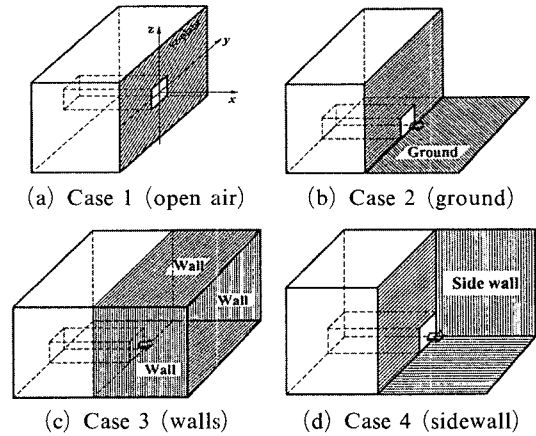

(a) Case 1 (open air)   (b) Case 2 (ground)

(c) Case 3 (walls)   (d) Case 4 (sidewall)

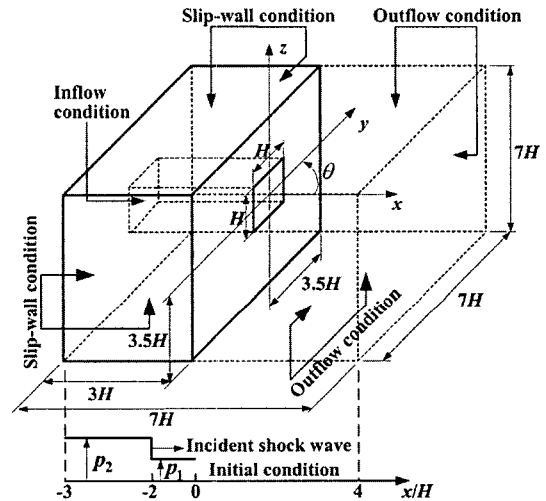**Fig. 1** Exit configurations of a square sectional duct

Fig. 2 Computational domain with boundary and initial conditions

outer boundaries, which are expressed as follows:

$$\sigma_{n-1}=\sigma_{i+1}, \ \sigma_n=\sigma_i : \text{Inflow condition} \quad (11)$$

$$\sigma_i=\sigma_n=\sigma_{n+1} \quad : \text{Outflow condition} \quad (12)$$

where σ is flow quantities such as pressure, density, velocity, etc., and the subscripts i and n refer to the inner grid and imaginary outer grid, respectively. A slip-wall boundary condition is applied to all of the solid walls, including the ground and sidewall. As an initial condition, an initial shock wave with the shock Mach number M_s begins to propagate from a position of $x'=-1.0$ inside the duct towards the exit. For testing
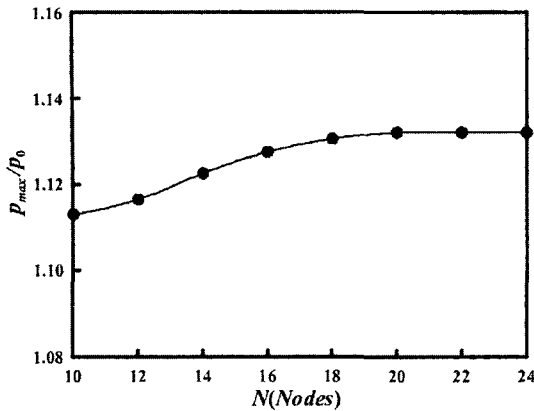
Fig. 3 Maximum pressure vs. nodes based on H

conditions, M_s was changed from 1.1 to 1.5. In order to examine the directivity of a propagating impulsive wave, pressure data have been obtained for several values of θ, which is an angle measured from the duct axis in the xy-plane.

Figure 3 shows the result of the preliminary test to find grid independent solution. The present computational grid system are built up using square cells with a constant size, which is decided by H/N where N is nodes applied to the height of the duct exit. For Case 1 at M_s=1.2, r/D=2.0 and θ=0°, the maximum pressure (p_{max}) given here is the highest peak pressure in a pressure-time history obtained as N increases up to 24. In this test, with a grid density over $\Delta x=\Delta y=\Delta z=H/20$, no significant changes in the accuracy of the solutions obtained have been found. The grid system was, therefore, set up with the grid density ($\Delta x=\Delta y=\Delta z=H/20$) and the resulting grid size is about 0.9 to 2.7 million nodes, depending on the exit configurations shown in Fig. 1.

3. Results and Discussion

For Case 1 at M_s=1.29, Fig. 4 shows the visualisation of wave propagation into the atmosphere with time obtained at the duct exit in the yz-plane. The static pressure contours predicted by the present CFD method (Fig. 4(b)) are compared with the interferograms (Fig. 4(a)) obtained by Jiang et al. (1999). The wave propaga-

$t = 20\mu s$

$t = 40\mu s$

$t = 60\mu s$

(a) Experiment   (b) Present CFD
(Jiang et al., 1999)
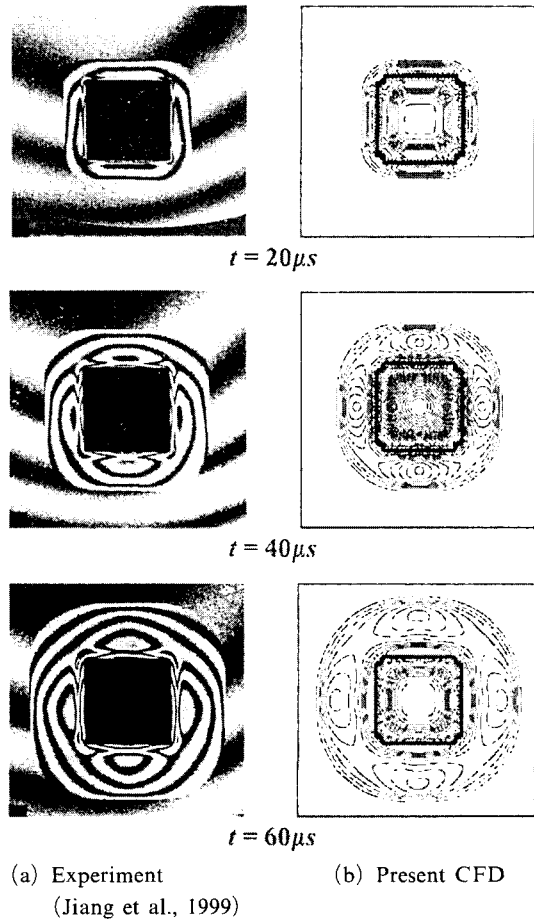
Fig. 4 Interferograms and computed pressure contours in the yz-plane (Case 1, M_s=1.29)

tion inside the duct was not visualised in the experiment while it is also presented in the CFD results. In both interferograms and iso-pressure contours, the inner and outer loops with rounded corners formed around the duct exit result from vortex generation and impulsive wave propagation, respectively. The pressure distribution inside the inner loop in the CFD results is due to the propagation of expansion waves towards the upstream in the duct. As time increases, the impulsive wave initially discharged from the duct at about t=20 μs propagates into the surrounding atmosphere with further rounded corners and shorter straight edges while the vortices develop without a typical pattern like the impulsive wave propagation. It implies that the vortices

developing around the duct exit have more sig-
nificant three-dimensional behaviour, compared
with the axisymmetric propagation of the im-
pulsive wave. At each instant, the present CFD
code gives a fairly good prediction of the boun-
dary shape of the impulsive wave as well as its
distribution. A slightly asymmetrical wave struc-
ture can, however, be observed in the experi-
mental results. It is mainly attributed to the opti-
cal setup employed in the experiment where an
object beam illuminated a flange surface sur-
rounding the duct exit with a small angle from the
duct axis (Jiang et al. 1999).

Another result for code validation is given in
Fig. 5, which shows maximum pressure values
obtained with a change in M_s at $r/D=2.0$ and
$\theta=0°$. The measured (Kashimura et al., 1999)
and computed maximum pressure values are in
good accordance quantitatively as well as quali-
tatively, which shows an almost linear increase
in p_{max} with increased M_s. From Fig. 4 and 5,
therefore, it is considered that the present CFD
analysis may provide proper simulations of im-
pulsive wave propagation from a duct.

For Case 2 at $M_s=1.2$, the static pressure con-
tours shown in Fig. 6 explain the physics of an
impulsive wave under ground effects, propagating
downstream of the duct. In order to provide an
understanding of the physics, three-dimension-
al pressure plots presented with static pressure
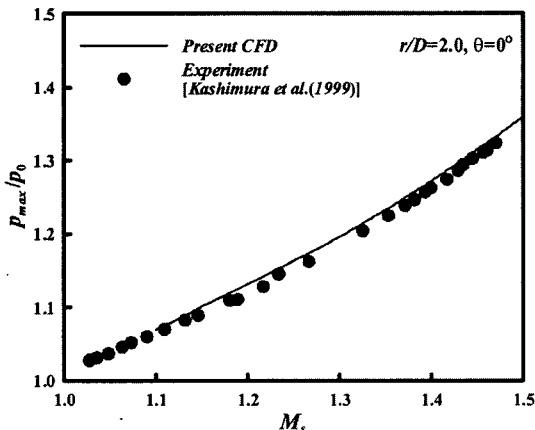
values, normalised by the atmospheric pressure,
are also given corresponding to the contours. In
the pressure plots, convex and concave regions
represent the propagating impulsive wave and
the vortical flow developing from the duct exit,
respectively. As time passes, the vortex loop be-
comes enlarged and the impulsive wave spreads
over a wider area with weaker strength. A fur-
ther rounded shape of the outer loop in the z-
direction indicates that the impulsive wave tends
to propagate into the upward space due to the
ground effects. In this situation, stronger pressure
gradients can be observed near the ground.

Figure 7 shows the pressure contours and
three-dimensional pressure plots obtained for
Case 3 at $M_s=1.2$. Until $t'=1.95$, an impulsive
wave has not reached the walls enclosing the
near field of the flow discharged from the duct
and the characteristics of wave propagation is
very similar to those of Case 2. At $t'=2.63$, the
impulsive wave is reflected from the walls and
propagates back towards the duct axis. Compar-
ed with Case 1 and Case 2, the interaction be-
tween the reflected shock and the waves pro-
pagating towards the walls leads to a more com-
plicated flow structure near the duct exit.

In Fig. 8, at the same initial condition, the
exit configuration of Case 4 results in a reduced
space of wave propagation to approximately
1/4 of Case 1 (1/2 of Case 2) by the influence of
the ground and sidewall, which partially block
the wave propagation in the yz-plane. Observing
each figure set, especially at $t'=1.24$, it is consi-
dered that the impulsive wave has relatively no-
ticeable directivity in the axial direction and
stronger vortices develop from the duct exit when
compared with other cases.

At $M_s=1.2$, Fig. 9 shows pressure histories
with time, obtained at the locations of $\theta=0°$,
$-45°$ and $-90°$ with a distance of $x'=2.0$, where
a negative value of θ denotes an angle measured
clockwise from the duct axis. For $\theta=0°$ (Fig. 9
(a)), static pressure changes in a similar trend
except Case 3. The pressure suddenly rises at
about $t'=1.50$ as an impulsive wave arrives at
the location and then decreases rapidly due to
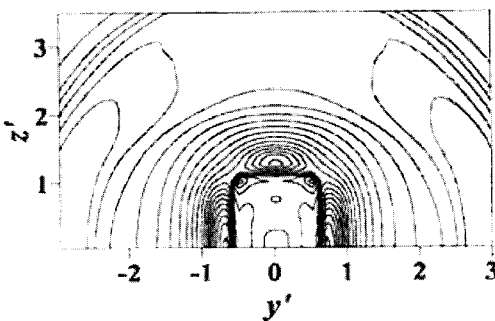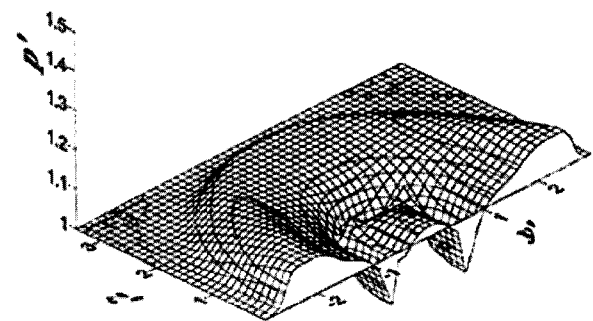ensuing flow expansion. Especially, in Case 3, a

Fig. 5 Computed and measured maximum pressure
vs. M_s (Case 1)
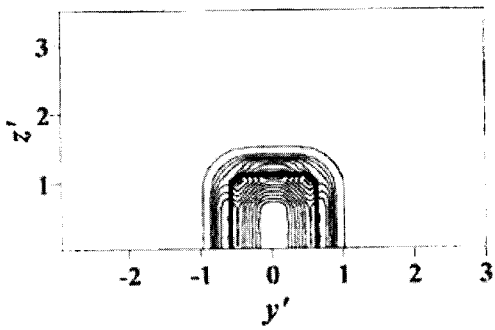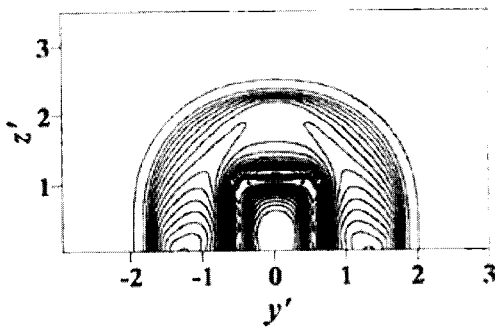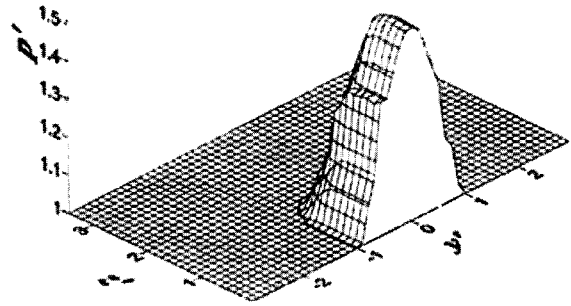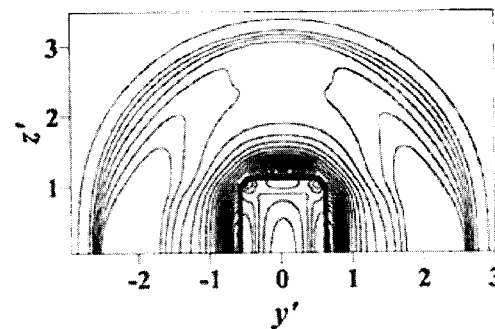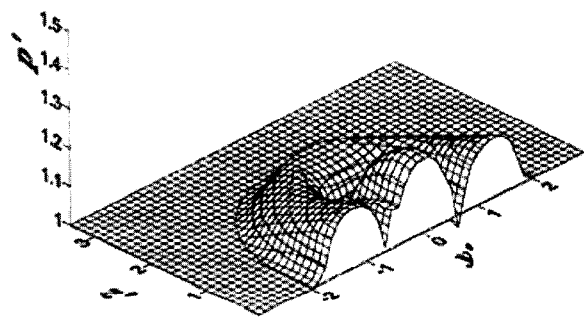
(a) $t'=0.49$
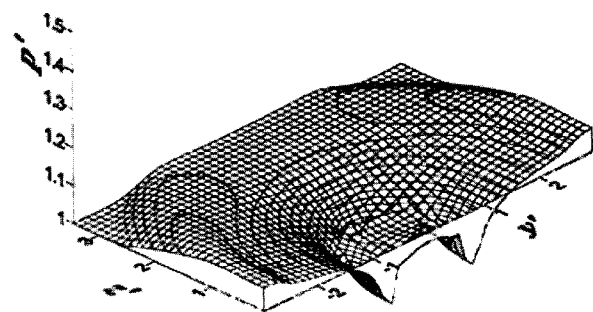
(b) $t'=1.24$

(c) $t'=1.95$

(d) $t'=2.63$

Fig. 6   Pressure contours in the yz-plane (Case 2, $M_s=1.2$)
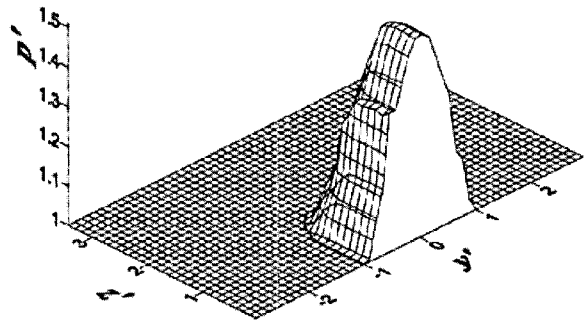
(a) $t'=0.49$

(b) $t'=1.24$

(c) $t'=1.95$

(d) $t'=2.63$

Fig. 7 Pressure contours in the yz-plane (Case 3, $M_s=1.2$)
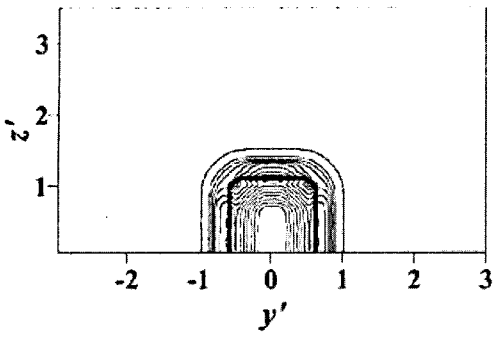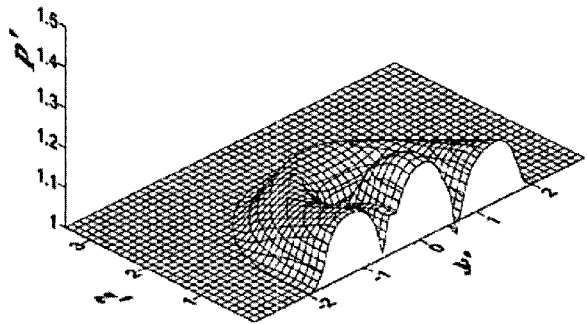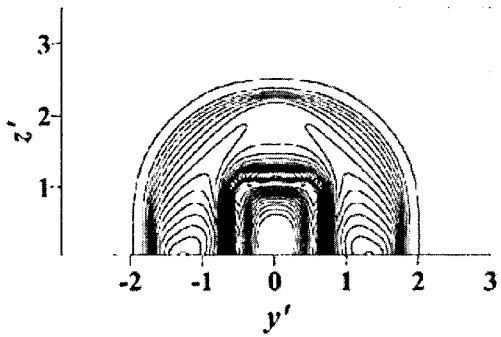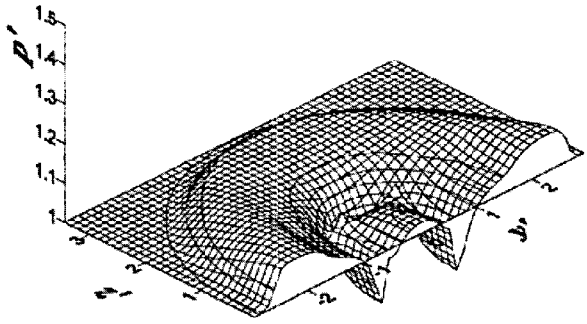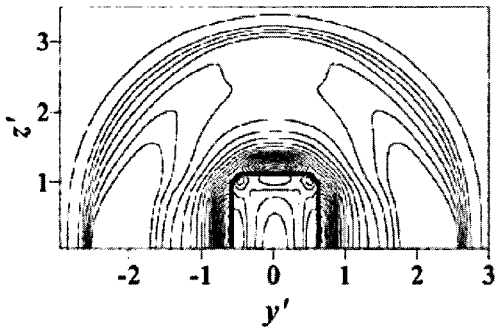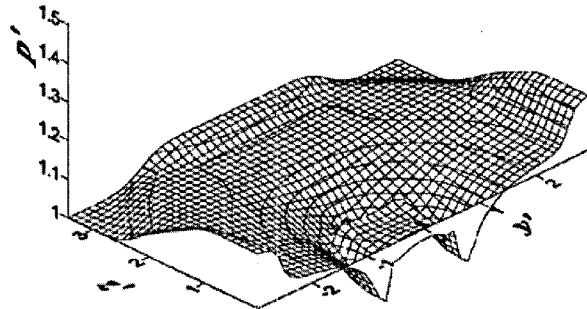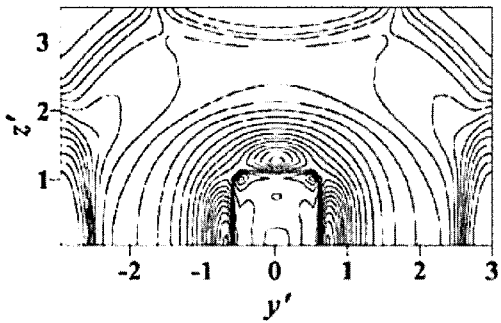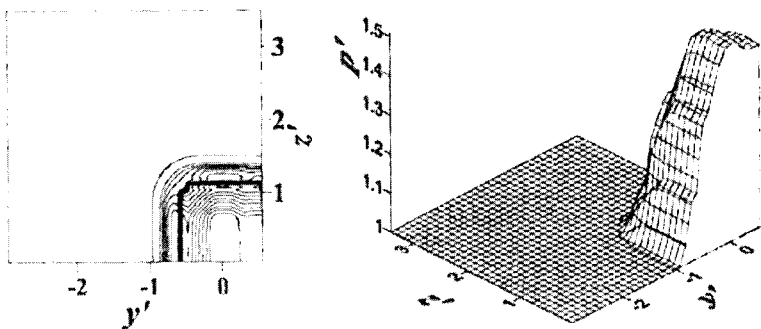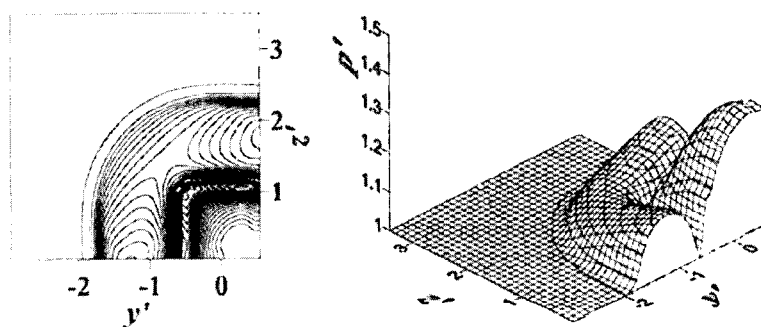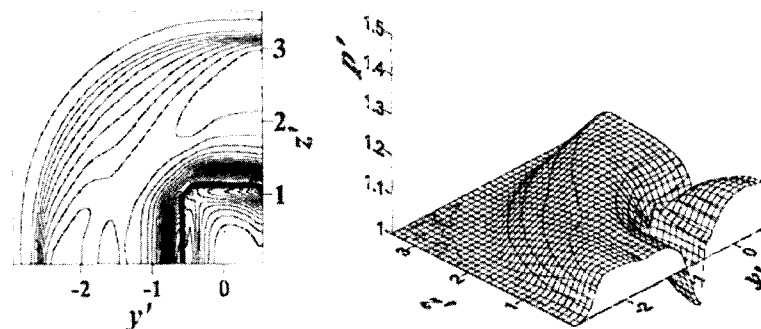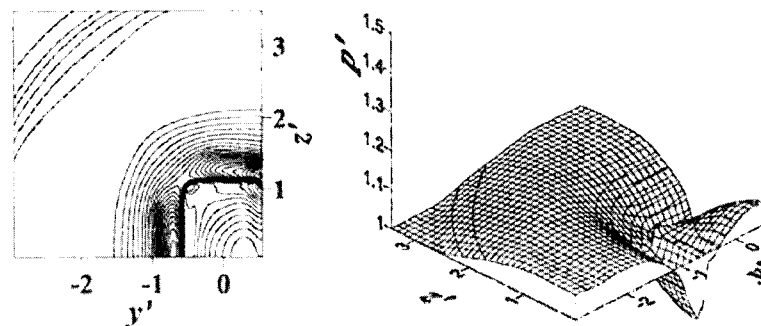
(a) $t'=0.49$

(b) $t'=1.24$

(c) $t'=1.95$

(d) $t'=2.63$

Fig. 8 Pressure contours in the yz-plane (Case 4, $M_s=1.2$)

secondary peak pressure value can also be observed at about $t'=4.40$ and it is attributed to the reflection of the shock towards the duct axis in the presence of the walls surrounding the discharging flow. For the exit configurations of the duct tested in the present computations, Case 4 gives the largest primary peak pressure value in the duct axis direction $(\theta=0°)$. For $\theta=-45°$ and $-90°$, where an estimation point is at a distance from

the axis (Fig. 9(b) and Fig. 9(c)), Case 3 has multiple peak pressure values and the primary peak pressure values of Case 2, Case 3 and Case 4 are observed to be almost same, dissimilar to the result obtained at the location where $\theta=0°$.

Figure 10 shows the effect of the existence of the ground and walls on the directivity of impulsive wave propagation. For $x'=1.0$ (Fig. 10 (a)), the maximum pressure of Case 1 is shown to be lower than those of other cases in all directions tested. For the other cases, Case 4 has the largest
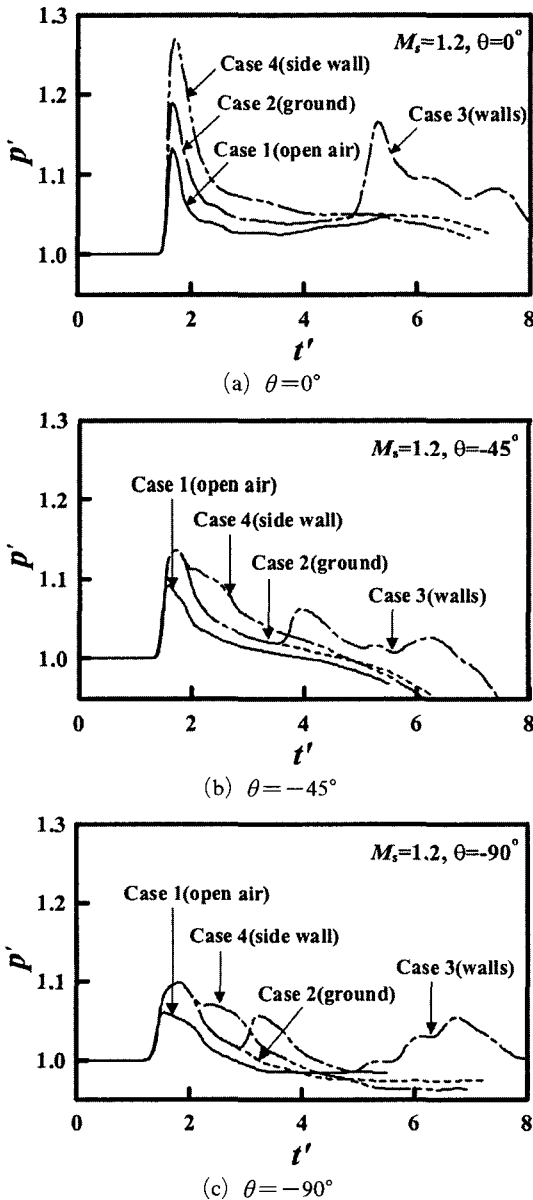

(a) $\theta=0°$

(b) $\theta=-45°$

(c) $\theta=-90°$

Fig. 9 Pressure histories in the xy-plane at $x'=2.0$
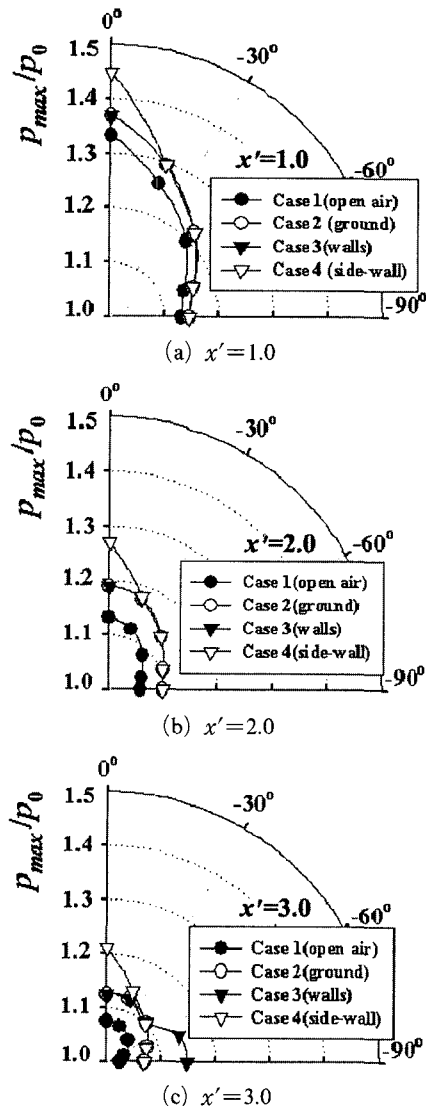

(a) $x'=1.0$

(b) $x'=2.0$

(c) $x'=3.0$

Fig. 10 Directivity of impulsive wave propagation $(M_s=1.2)$

maximum pressure at $\theta = 0°$ while the influence of the exit configuration on the maximum pressure becomes negligible as the angle increases. The directivity of impulsive wave propagation for $x' = 2.0$ (Fig. 10(b)) is observed to be qualitatively very similar with that for $x' = 1.0$. At the locations with this distance, however, the differences in the values between Case 1 and the others are more significant. It implies that the existence of the ground and walls leads to lesser dissipation of the impulsive wave. For $x' = 3.0$ (Fig. 10 (c)), a different characteristic of wave propagation can be seen. The maximum pressure of Case 3 becomes the largest at a given location of $\theta > |-45°|$, which is close to walls, due to the effect of shock reflection from the walls. From the results, it is considered that the peak pressure value decreases in all directions as the impulsive wave propagates away from the duct exit and an exit configuration like Case 4 has the most significant axial directivity of wave propagation amongst the configurations tested in this CFD study.

Figure 11 shows the effect of the Mach number of an initial shock wave on the peak pressure under the exit configuration of Case 3, in terms of the difference between primary and secondary peak pressure values normalised by the atmospheric pressure. A typical pressure history of Case 3 at a location in the duct axis is given in Fig. 11 (a). In this case, generally, there are two peak values observed at $\theta = 0°$. A largest peak pressure is generated as the initial shock wave reaches a given location and pressure increases sharply again when the shock propagates back to the duct axis after reflection. As shown in the figure, the peak pressure values are defined by $\Delta p_{max,1}$ and $\Delta p_{max,2}$, respectively, which are the pressure differences between peak values and a base value (atmospheric pressure). For $x' = 1.0$ and 2.0, as M_s increases, the peak pressure difference becomes larger. With a further increase in distance ($x' = 3.0$), primary and secondary peak values are almost same for M_s up to 1.2 but there is a range of M_s at which the secondary peak value is slightly larger than the primary one. It implies that the influence of the reflected shock on the
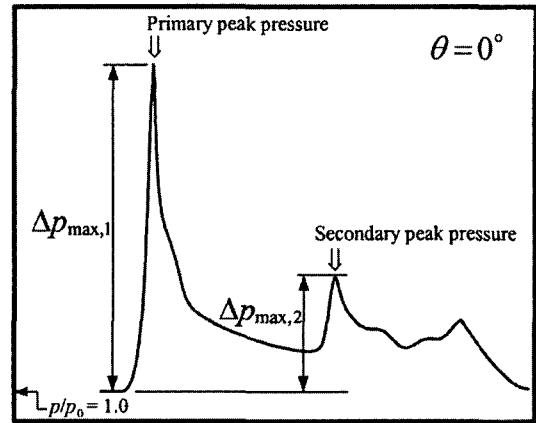
(a) Typical pressure history of Case 3 in the duct axis direction
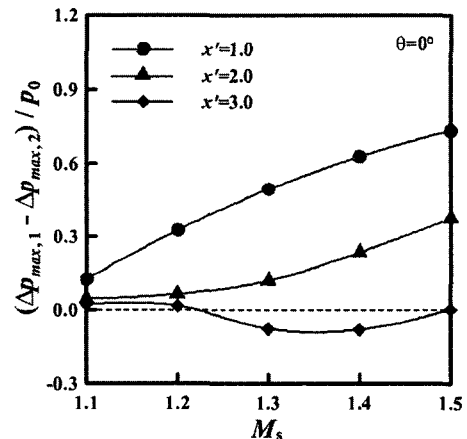
(b) Difference between primary and secondary peak pressure values

Fig. 11 Peak pressure vs M_s (Case 3, $\theta = 0°$)

main flowfield may become significant in a specific range of M_s. It is also noted that a change in the peak pressure difference in the longitudinal direction is relatively severe with a larger M_s. To effectively alleviate impulsive noise and vibration problems, therefore, the characteristics of impulsive wave propagation under ground and walls effects should be understood in consideration of the range of the initial shock Mach number which is obtained in a given situation.

4. Conclusions

The present paper describes the physics included in the unsteady flow characterised by an

impulsive wave discharged from a square cross-sectional duct, using a numerical method. To correctly predict the unsteady impulsive wave propagation, the Yee-Roe-Davis's TVD scheme was applied to three-dimensional, unsteady, compressible Euler equations. The results obtained showed that the propagation of an impulsive wave strongly depends on the Mach number of an initial shock wave and the exit configurations of the duct under consideration. Especially, in the presence of the ground, single sidewall and walls, the longitudinal directivity of impulsive wave propagation became more remarkable. Concerning four different exit configurations employed in the present computational analysis, the case with the ground-sidewall led to the largest peak pressure value in the duct axis direction. For the case with the ground-walls, multiple peak pressure values were observed in pressure histories due to the reflection of the impulsive wave from the walls. For this exit configuration, in the region close to the walls, the maximum pressure became larger than the other cases. From the results obtained, it is considered that a detailed understanding of specific characteristics of the impulsive wave propagation formed downstream of a given exit configuration of a flow passage is indispensable to effectively reduce the impulsive noise and vibrations or to improve the performance of pulse devices.

Acknowledgment

References

Britan, A. B., Rudnitskii, A. Ya. and Starik, A. M., 1988, "Numerical Modeling of Reflection of a Shock Wave at a Wall with an Aperture," *High Temp.*, Vol. 25, No. 5, pp. 712~718.

Cooke, C. H. and Fansler, K. S., 1989, "Comparison with Experiment for TVD Calculations of Blast Waves from a Shock Tube," *Intl. J. Numer. Meth. Fluids*, Vol. 9, No. 1, pp. 9~22.

Fox, J. A. and Vardy, A. E., 1973, "The Generation and Alleviation of Air Pressure Transients Caused by the High Speed Passage of Vehicles Through Tunnels," *Proc. 1st International Symposium on Aerodynamics and Ventilation of Vehicle Tunnels*, pp. G3.49~G3.64.

Jiang, Z., Onodera, K. and Takayama, K., 1999, "Evolution of Shock Waves and the Primary Vortex Loop Discharged from a Square Cross-Sectional Tube," *Shock Waves*, Vol. 9, pp. 1~10.

Kashimura, H., Setoguchi, T., Kim, H. D., Kweon, Y. H. and Matsuo, K., 1999, "Emission of a Propagating Shock Wave from an Open End of a Tube," *Transaction of the JSME, Part B*, Vol. 65, No. 633, pp. 1665~1670.

Kentfield, J. A. C., 1993, *Nonsteady, One-Dimensional, Internal, Compressible Flows (Theory and Applications)*, Oxford University Press, Oxford, Ch. 7.

Kim, H. D., Kweon, Y. H., Aoki, T. and Setoguchi, T., 2004, "A New Technique for the Control of a Weak Shock Discharged from a Tube," *IMechE Part C : J. Mechanical Engineering Science*, Vol. 218, pp. 377~387.

Kim, H. D., Kweon, Y. H. and Setoguchi, T., 2003, "A Study of the Impulsive Wave Discharged from Inclined Exit of a Tube," *IMechE Part C : J. Mechanical Engineering Science*, Vol. 217, No. 2, pp. 271~279.

Kim, H. D., Lee, D. H., Kashimura, H. and Setoguchi, T., 2003, "Propagation Characteristics of Compression Waves Reflected from the Open End of a Duct," *KSME Intl. J.*, Vol. 17, No.5, pp. 718~725.

Kim, H. D. and Setoguchi, T., 1999, "Study of the Discharge of Weak Shocks from an Open End of a Duct," *J. Sound and Vibration*, Vol. 226, No. 5, pp. 1011~1028.

Kim, H. D., Setoguchi, T., Kweon, Y. H., Miura, S. and Kashimura, H., 1998, "Studies on Reflection of Weak Shock Waves from an Open End of a Tube with Baffle Plate," *Proc. 11th International Symposium on Transport Phenomena (ISTP-11)*, pp. 94~99.

Klingel, R. and Löffler, F., 1983, "Dust Collection and Cleaning Efficiency of a Pulse Jet

Fabric Filters," *Filtration and Separation*, Vol. 20, pp. 205~208.

Klingenberg, G. and Heimerl, J. M., 1992, "Gun Muzzle Blast and Flash," *Progress in Astronautics and Aeronautics*, AIAA Educational Series, American Institute of Aeronautics and Astronautics.

Kweon, Y. H., Kim, H. D., Setoguchi, T. and Aoki, T., 2003, "A Study of the Impulse Wave Discharged from the Exits of Two Parallel Tubes," *J. Thermal Science*, Vol. 12, No. 4, pp. 332~336.

Matsuo, K. and Aoki, T., 1992, "Wave Problems in High-Speed Railway Tunnels," *Proc. 18th International Symposium on Shock Tube and Waves* (Ed. Takayama, K.).

Ozawa, S., Maeda, T., Matsumura, T., Uchida, K., Kajiyama, H. and Tanemoto, K, 1991, "Countermeasures to Reduce Micro-Pressure Waves Radiating from Exits of Shinkansen Tunnels," *Proc. 7th International Symposium on the Aerodynamics and Ventilation of Vehicle Tunnels*, Brighton.

Pennelegion, L. and Grimshaw, J. F., 1979, "The Diffraction of the Blast Wave Emerging from a Conical Nozzle Driven by Compressible Gas," *Proc. 12th International Symposium on Shock Tubes and Waves*, pp. 349~358.

Raghunathan, S., Kim, H. D. and Setoguchi, T., 1998, "Impulse Noise and Its Control," *Prog.*

Aerospace Sci., Vol. 34, No. 1, pp. 1~44.

Rudinger, G., 1955, "Improved Wave Diagram Procedure for Shock Reflection from an Open End of a Duct," *J. Appl. Physics*, Vol. 26, No. 11, pp. 1339~1341.

Rudinger, G., 1957, "The Reflection of Pressure Wave of Finite Amplitude from an Open End of a Duct," *J. Fluid Mechanics*, Vol. 3, No. 1, pp. 48~66.

Sekine, N., Matsumura, S., Aoki, K. and Takayama, K., 1989, "Generation and Propagation of Shock Waves in the Exhaust Pipe of a Four Cycle Automobile Engine," *Proc. 17th International Symposium on Shock Wave and Shock Tube*, pp. 671~676.

Setoguchi, T., Matsuo, K., Hidaka, F. and Kaneko, K., 1993, "Impulsive Noise Induced by a Weak Shock Wave Discharged from an Open End of a Tube," *Acoustic Characteristics and Its Passive Control*, American Society of Mechanical Engineers, New York, FED-Vol. 170, pp. 57~64.

Sod, G. A., 1977, "A Numerical Study of a Converging Cylindrical Shock," *J. Fluid Mechanics*, Vol. 83, pp. 785~794.

Yee, H. C., 1987, "Upwind and Symmetric Shock Capturing Schemes," *NASA TM*-89464.

Zinn, B. T., 1985, "Pulsating Combustion," *Trans. ASME, Mech. Engng.*, Vol. 107, No. 8, pp. 36~41.